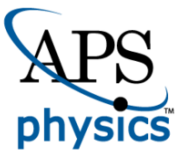



# Scaling and Diabatic Effects in Quantum Annealing with a D-Wave Device

Phillip Weinberg, Marek Tylutki, Jami M. Rönkkö, Jan Westerholm, Jan A. Åström, Pekka Manninen, Päivi Törmä, and Anders W. Sandvik

Phys. Rev. Lett. **124**, 090502 — Published 5 March 2020

DOI: 10.1103/PhysRevLett.124.090502

# Scaling and diabatic effects in quantum annealing with a D-Wave device

Phillip Weinberg,[1] Marek Tylutki,[2,3] Jami M. Rönkkö,[4] Jan Westerholm,[5]
Jan A. Åström,[4] Pekka Manninen,[4] Päivi Törmä,[2] and Anders W. Sandvik[1,6]

[1]*Department of Physics, Boston University, 590 Commonwealth Avenue, Boston, Massachusetts 02215, USA*
[2]*Department of Applied Physics, Aalto University School of Science, FI-00076 Aalto, Finland*
[3]*Department of Physics, Warsaw University of Technology, ul. Koszykowa 75, 00-662 Warsaw, Poland*
[4]*CSC–IT Center for Science, P.O. Box 405, FIN-02101 Espoo, Finland*
[5]*Faculty of Science and Engineering, Åbo Akademi University, Vattenborgsvägen 3, FI 20500, Åbo, Finland*
[6]*Beijing National Laboratory of Condensed Matter Physics and Institute of Physics, Chinese Academy of Sciences, Beijing 100190, China*

(Dated: February 10, 2020)

We discuss quantum annealing of the two-dimensional transverse-field Ising model on a D-Wave device, encoded on $L \times L$ lattices with $L \leq 32$. Analyzing the residual energy and deviation from maximal magnetization in the final classical state, we find an optimal $L$ dependent annealing rate $v$ for which the two quantities are minimized. The results are well described by a phenomenological model with two powers of $v$ and $L$-dependent prefactors to describe the competing effects of reduced quantum fluctuations (for which we see evidence of the Kibble-Zurek mechanism) and increasing noise impact when $v$ is lowered. The same scaling form also describes results of numerical solutions of a transverse-field Ising model with the spins coupled to noise sources. We explain why the optimal annealing time is much longer than the coherence time of the individual qubits.

The prospect of simulating theoretical quantum many-body Hamiltonians with controllable engineered systems is now an important motivation for atomic and quantum device physics [1–3]. Systems explored for creating such "synthetic quantum matter" include ultracold gases [4–9], photonic devices [10–14], polaritons [15], and trapped ions [16–22]. Another emerging simulation platform is large arrays of superconducting qubits [23–28], which were originally envisioned in the context of quantum annealing (QA) as efficient solvers of classical optimization problems mapped to Ising like Hamiltonians [29–42]. To reach the classical ground state (the problem solution) in a QA process, strong quantum fluctuations are initially induced by applying a transverse field, which is quasi-adiabatically reduced to zero. QA devices operating according to this principle have entered industrial production and applications beyond the academic setting [23], motivated by the hope of more efficient solutions of NP-hard problems [32, 43] and, more recently, quantum enhanced machine learning [44, 45]. It is still unclear what systems (classes of optimization problems) are amenable to significant speedup, and to what extent QA can be realized in actual devices [40, 46–54].

While the question of quantum speedups is essential, the potential of using QA devices as generic quantum many-body emulators motivates a broader range of investigations into the devices and how they can be exploited for probing various quantum phenomena. As an example, recently a QA device produced by D-Wave Systems was used in an impressive study of a quantum phase transition of a quantum spin glass [28]. An important question in applications of QA devices, for optimization or quantum simulation, is whether the desired adiabatic evolution is sufficiently realized in the presence of noise (the environment) and finite annealing time. This question motivates studies of the dependence of measured properties on the annealing time [26, 55–58], which also impacts the effects of noise. For this purpose, it may be particularly fruitful to implement simple, uniform model Hamiltonians to avoid distractions of not fully understood random couplings [59]. Such a study was already carried out with the one-dimensional transverse-field Ising model (TFIM) coded on a D-Wave device [58], but the results did not exhibit any obvious scaling behavior.

In this Letter, we report success of a scaling approach for a two-dimensional (2D) Ising model, with data generated on the D-Wave `DW_2000Q_2_1` solver (DWQ) [23]. We observe how the improved adiabaticity with lowered

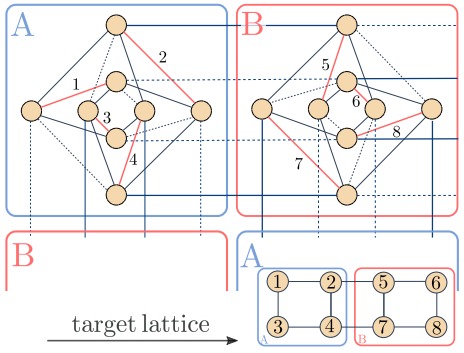


FIG. 1. Illustration of the DWQ Chimera graph and the embedding of our target open square Ising lattice (upper left corner shown). The red links show how the physical qubits are coupled with $J_{\rm HC}$ to create the logical qubits of the target model. The solid and dashed lines correspond to the active and inactive couplings, respectively. The embedding requires two types of Chimera patterns that tile the plane like a chess board. See SM for details [61].

annealing rate competes with diabatic noise mechanisms causing opposite effects, leading to an optimal annealing rate. We introduce a unified scaling ansatz which can account phenomenologically for both mechanisms in the DWQ and also describes numerical results for QA of a model Hamiltonian with external noise.

*Model Embedding.*—The DWQ device emulates the TFIM with an array of superconducting loops which form qubits corresponding to spin-1/2 operators $\sigma_i$ (Pauli matrices). The "Chimera" interaction graph is made out of cells of eight qubits, each connected to six other qubits (five on the graph boundary) and a longitudinal field $h_i$, thus realizing an Ising Hamiltonian of the form $\mathcal{H}_{\rm class} = \sum_{\langle ij\rangle} J_{ij}\sigma_i^z\sigma_j^z + \sum_i h_i\sigma_i^z$. Here $J_{ij}$ and $h_i$ are dimensionless couplings with values in $[-1,1]$. All qubits are coupled to a transverse field, which along with the overall interaction strength is varied through a time-dependent parameter $s(t) \in [0,1]$ for a total Hamiltonian

$$\mathcal{H}_{\rm TFIM} = A(s)\sum_i \sigma_i^x + B(s)\mathcal{H}_{\rm class}. \qquad (1)$$

$A(s)$ and $B(s)$ are smooth non-linear functions of $s$ [24, 26, 28] such that $B(0) = 0$ initially and $A(1) = 0$ at the end of the QA process. Within these bounds there is some flexibility in $s(t)$. The total annealing time can be varied from microseconds to milliseconds.

For geometries that do not fit on the Chimera graph, logical qubits can be created by coupling two or more physical qubits together with a "high-cost" coupling [60], $-J_{\rm HC} = 1$, to keep their values mostly the same. The logical qubits can then be coupled in more complicated geometries [28, 52, 58]. Here we realize $L \times L$ open-boundary lattices (tiles) by using logical qubits constructed from two physical qubits; see Fig. 1 and Supplemental Material (SM) [61]. Our target model has equal nearest-neighbor ferromagnetic couplings $J_{ij} = -J_{\rm Ising}$ and $h_i = 0$. The DWQ has 2048 qubits, and the maximum lattice size for our target model is hence $32 \times 32$. Smaller tiles are implemented by appropriately zeroing some couplings, and for $L \leq 16$ we can study several tiles in parallel. The device typically has some nonfunctioning qubits, and we treat all logical qubits affected by defects as vacancies, completely isolating them by zeroing coupling. The number of vacancies is typically at most a few percent, and tiles with an excessive number of vacancies are not included in the analysis.

We use the maximum high-cost coupling in units of frequency, $J_0 = B(1)J_{\rm HC}/\hbar \approx 2$ GHz [60], to set the time units in our plots. Our aim is to study the final-state excitation energy and magnetization as functions of the annealing time $T$. To this end, we chose the simplest possible protocol—a linear ramp with $s(t) = t/T = vtJ_0$, with the dimensionless velocity $v = 1/(TJ_0)$.

*Phase transition and bath effects.*—The 2D TFIM with Ising coupling $J$ and field $h_x$ undergoes a phase transition between ferromagnetic and paramagnetic ground states at $h_x/J \approx 3.04$. Thus, in the DWQ embedded model we expect a phase transition for some value of $s$ that also depends on $A(s)$ and $B(s)$ in Eq. (1). The system will traverse the quantum critical point on its way to the final ordered ferromagnetic classical state, and this point, where the excitation gap has a size-dependent minimum, is the bottleneck for the system to remain in the instantaneous ground state during the entire QA process.

Both classical (stochastic dynamics) and quantum (Hamiltonian dynamics) systems exhibit dynamic scaling in the velocity by which a parameter changes when passing through a critical point sufficiently slowly. In the neighborhood of the phase transition the exponents are predicted by the Kibble-Zurek mechanism (KZM) [62–65] and its generalization as an out-of-equilibrium finite-size scaling (FSS) ansatz [59, 66–72]. As an example, the residual Ising energy, defined as $\Delta_E = \mathcal{H}_{\rm class} - E_{\rm I}$, where $E_{\rm I}$ is the Ising energy in the instantaneous ground state, scales as (in $d$ dimensions with correlation-length exponent $\nu$ and dynamic exponent $z$) $\Delta_E \sim \xi_{\rm KZ}^{-d} \sim L^d v^{\nu d/(1+\nu z)}$, where $\xi_{\rm KZ}$ is the freeze-out length [62–65]. However, in the long-time limit it has been argued that the Landau-Zener mechanism (LZM) applies, where adiabatic evolution is only controlled by the minimum gap $\Delta_L \sim L^{-z}$, giving $\Delta_E \sim L^d v^{1/2z}$ [35, 38, 39, 41, 42, 63]. Other types of dynamics, e.g., quantum coarsening, may also play a role in the long-time limit [73, 74].

The KZM and LZM assume an isolated system, but in a device there is always some coupling to a bath or other sources of noise. Works on QA in open quantum systems have discussed decoherence due to defects produced by the environment at a rate determined by the temperature and the couplings to the system [75–77]. If the bath induced defect density remains low throughout the QA process, there may still be a regime where the scaling depends on the critical point as in the KZM or LZM. However, in some cases the bath can lead to new power laws [78] or destruction of the critical point [79, 80]. Decoherence can also some times assist the QA process in approaching the classical ground state [55, 81–83]. Given the desire to better understand and characterize the QA process, we will present a systematic FSS analysis of annealing data obtained with the DWQ device.

*Results.*—We investigate the excess energy $\Delta_E$ and the deviation of the magnetization from its maximal (absolute) value $N$ (the number of qubits), $\Delta_M = N - |\sum_i \sigma_i^z|$. We saw no significant difference between observables calculated from the logical qubits versus the physical qubits, reflecting the rarity of violations of the $J_{\rm HC}$ constraint. Here we present results for the physical qubits on the Chimera graph. In the DWQ device a projective measurement is performed at the end of each annealing run, returning a product state in the $\sigma^z$ basis. We repeat the annealing protocol at least $2 \times 10^4$ times (over multiple days) and average over the final configurations.

In Fig. 2 we show results from the DWQ with $J_{\rm Ising} =$

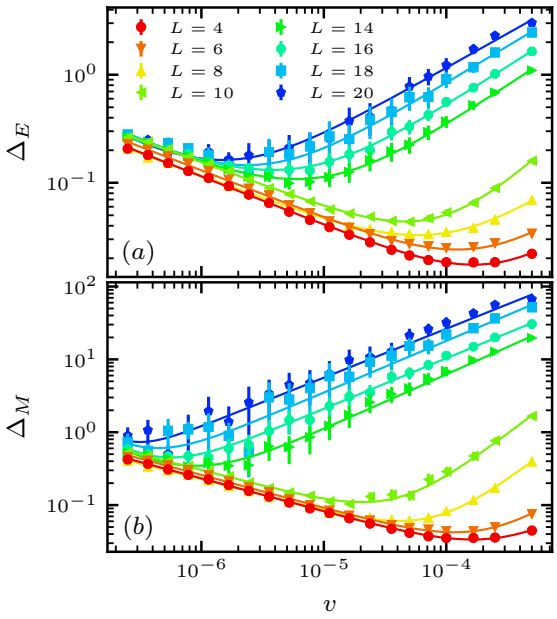


FIG. 2. Mean values of the excess energy (a) and the magnetization deficit (b) for different lattice sizes after DWQ annealing runs with $J_{\rm HC}$ set to the maximum possible value [60] and $J_{\rm Ising} = 0.5 J_{\rm HC}$. Each point was calculated using averages of at least $2 \times 10^4$ independent measurements. The curves are fits to Eq. (2). The case $L = 12$ was not studied.

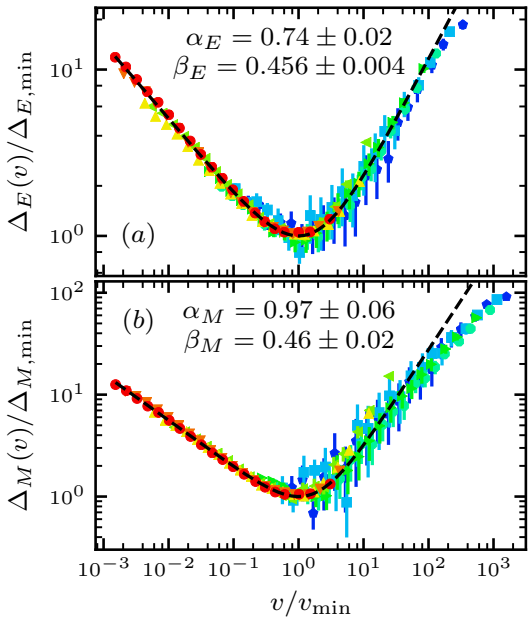


FIG. 3. Scaling collapse of the data from Fig. 2. The curves represent fits to Eq. (3) for $L$ = 10-20, giving the exponents $\alpha$ and $\beta$ for the two quantities shown in the respective panels.

0.5 (see SM [61] for the motivations for this choice) and lattice sizes up to $L = 20$. We have carried out runs up to $L = 32$ (see SM [61]), but we excluded the larger systems here because of large statistical fluctuations and no distinct minimums in the accessible velocity window. For the smallest systems, in Fig. 2 we see that $\Delta_E$ and $\Delta_M$ are already close to their smallest attainable values at the highest $v$, and upon reducing $v$ both quantities increase. Clearer minimums (optimal velocities) form and shift to lower velocities as $L$ increases. We find power laws emerging on both sides of the minimums. An optimal annealing rate is consistent with general expectations for QA in a system coupled to a heat bath or noise [75–77, 84–86], provided that the temperature or noise strength is not too high [87]. To our knowledge, the size dependence has not been discussed extensively.

A candidate for a phenomenological model to fit the data is simply a sum of two power laws:

$$f(v) = a_L v^{\alpha} + b_L v^{-\beta}, \tag{2}$$

and $a_L$, $b_L$, $\alpha$, and $\beta$ positive parameters (different for $f = \Delta_E$ and $f = \Delta_M$). The first term accounts for the defect production from non-adiabatic QA (which decreases as $v$ decreases), while the second term is the contribution of defects from the bath (which should increase as $v$ decreases [77]). As shown in Fig. 2, the form indeed fits all the data. For the larger systems $a_L$ scales as $L^2$ for both the energy and the magnetization (see SM [61]), which is consistent with both the KZM and LZM (extensive defect production). The prefactor $b_L$ of the bath term is almost independent of $L$ (as seen in the low-$v$ data in Fig. 2 and further analysis in SM [61]), where one might instead have expected an extensive contribution. This behavior may be an indication of highly non-uniform noise (see discussion in SM [61]) and calls for further investigations of the couplings of the DWQ qubits to the environment.

Even without detailed understanding of the noise, our proposed form (2) provides a way to quantify the competition between adiabatic and diabatic mechanisms. The optimal values $f_{\rm min}(L)$ for both the energy and the magnetization ($f_{\rm min} = \Delta_{E,\rm min}$ or $f_{\rm min} = \Delta_{M,\rm min}$) and the corresponding velocities $v_{\rm min}(L)$ can be used to define rescaled velocities and observables,

$$u \equiv \frac{v}{v_{\rm min}}, \qquad g(u) \equiv \frac{f(u v_{\rm min})}{f_{\rm min}} = \frac{\beta u^{\alpha} + \alpha u^{-\beta}}{\alpha + \beta}, \tag{3}$$

where the last form follows from Eq. (2); note the absence of the factors $a_L$ and $b_L$. In Fig. 3 we show the rescaled data along with fits to Eq. (3). The resulting exponents $\alpha$ and $\beta$ are displayed in Fig. 3. The QA exponents $\alpha_E$ and $\alpha_M$ agree remarkably well with the Ising KZM forms ($d = 2, z = 1, \nu \approx 0.630, \beta \approx 0.326$); $\Delta_E \sim v^{d\nu/(1+\nu)} \sim v^{0.77}$ and $\Delta_M \sim v^{(d\nu+\beta)/(1+\nu)} \sim v^{0.97}$ [59, 66–72] (see SM [61] for further discussion of the exponents). The LZM energy is $\Delta_E \sim v^{1/2}$ (and $\Delta_M$ is undetermined). The observed KZM scaling indicates that the accessible annealing times, before the cross-over to the noise regime, are still not in the long-time limit where

other mechanisms [73, 74] take over (see also SM [61]).

*Modeling the Bath.*—To understand the diabatic effects responsible for the second term in Eq. (2), we use a simple model of decoherence; the TFIM with a noisy transverse field (similar to Refs. [75, 76, 88]). Since calculations for 2D models are limited to very small systems, we use a 1D model to test the proposed generic scaling forms in Eqs. (2) and (3). We find qualitatively similar behaviors with a size-dependent optimal velocity. Note that the KZM predicts universal scaling in the velocity regime where the noise is not important, with exponents given by the relevant universality class and dimensionality (see SM [61]).

The Hamiltonian consists of coherent and noisy parts; $\mathcal{H}(t) = \mathcal{H}_0(t) + \mathcal{V}_{\rm noise}(t)$, where

$$\mathcal{H}_0(t) = -\left(\frac{t}{T}\right)^2 \sum_{i=1}^{L-1} \sigma_i^z \sigma_{i+1}^z - \left(1 - \frac{t}{T}\right)^2 \sum_{i=1}^{L} \sigma_i^x. \quad (4)$$

Here $T$ is the annealing time and the time dependence is similar to that in the DWQ. The noise couples to the transverse field of each qubit with strength $\lambda$,

$$\mathcal{V}_{\rm noise}(t) = \lambda \sum_i \eta_i(t) \sigma_i^x, \quad (5)$$

where $\eta_i(t)$ are classical fields representing the interaction with the environment [76]. Experiments run on the DWQ have found that the Ising interactions $J_{ij}$ exhibit noise with an approximate $1/\omega^p$ spectrum with $0.75 \lesssim p \lesssim 1$ [24, 60]. The physics is not significantly different when the noise is instead added to the transverse field [76], as we do here. The noise can be summarized with the following temporal and spatial correlations: $\langle \eta_i(t)\eta_j(t')\rangle = \delta_{ij} C(t-t')$, with $C(t-t')$ the autocorrelation function for the noise. We normalize the noise such that the standard deviation is set to unity and approximate $\eta_i(t)$ as a sum over $10^3$ cosines with frequencies sampled (see details in SM [61]) from a power-law spectrum $S(\omega)$ with a cutoff scale $\omega_0$;

$$S(\omega) = \frac{(\omega/\omega_0)^{-p} e^{-\omega/\omega_0}}{\omega_0 \Gamma(1-p)}. \quad (6)$$

We set $\omega_0 = 1$ (given in the natural units of $H_0$), the exponent to $p = 0.75$, and noise coupling $\lambda = 0.01$.

The simulation starts with the system in the ground state at $t = 0$, and the evolution with the Schrödinger equation is performed by a Jordan-Wigner transformation to fermions and solving the Bogoliubov-de Gennes equations [41, 75]. To calculate the expectation value of the energy from the density matrix, we perform many runs with different noise realizations and average over the expectation values calculated with the pure state at the end of the run. We did not compute $\Delta_M$, which would be more time consuming.

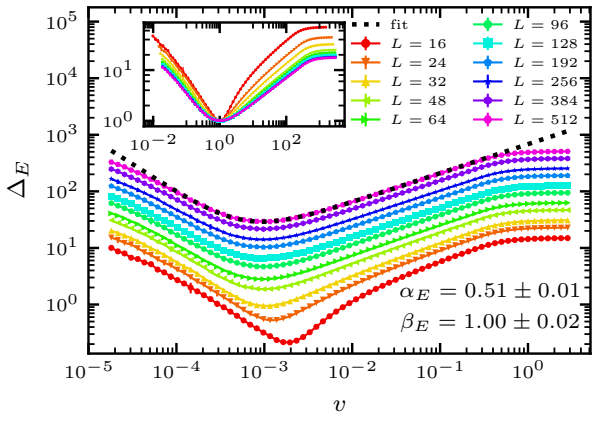


FIG. 4. Mean residual energy of the 1D TFIM at the end of QA simulations with noise described by Eq. (5) and parameters given in the text. The inset shows the data rescaled according to Eq. (3). A fit gives the exponents shown in the plot; the $L = 512$ form is shown as the dashed curve.

Figure 4 shows results for various chain lengths. The excess energy first decreases when $v$ is lowered but increases as $v \to 0$, similar to the DWQ (Fig. 2). The inset shows data collapse with the same kind of rescaling as with the DWQ data in Fig. 3. The prefactors $a_L$ and $b_L$ are both $\propto L$ (see SM [61]), i.e., the noise effects are extensive in this case. The KZM and LZM exponents are identical for this system, $\alpha = 1/2$, and $a_L \propto L$, and these power laws agree with the observations. At high $v$, where the system cannot evolve significantly, the rescaled data approach a constant, corresponding to the properties of the initial state. Interestingly, in the DWQ data (Fig. 3) we also observe similar deviations from the power law at the highest velocities, but there the values are still quite far from (about an order of magnitude) those of the ideal fully $x$ polarized initial state.

*Discussion.*—We have shown that QA in the DWQ and a prototypical model system both produce results captured by a simple scaling form, Eq. (2), with two power laws describing the competition between quasi-adiabatic annealing and diabatic effects of a bath. The size-dependent prefactors indicate whether defect production by the two sources is extensive or not, and the powers of the velocity contain information on the excitation mechanisms at play. Our model system exhibits extensive defect production, as expected, and the velocity scaling in the annealing regime is consistent with the KZM and LZM (which have the same exponents in the case of the 1D TFIM). In the DWQ, the velocity scaling is better described by the KZM than the LZM. The bath effects are subextensive, which may indicate highly non-uniform effects of the bath [61].

The optimal annealing time, in the DWQ and in the model, is much longer than the coherence time of an individual qubit. As we discuss further in SM [61], corre-

lations among the qubits lessen the impact of noise and lead to a longer collective time scale of domain ordering. The optimal annealing time should not be seen as a purely quantum mechanical coherence time, but reflects a fascinating interplay between quantum dynamics and stochastic processes that deserves further study.

Our scaling ansatz should be useful as a generic tool for quantifying QA in the presence of noise sources and baths. In future experiments with QA devices, it would be interesting to regulate the coupling to the environment in some way, e.g., by changing the temperature of the system or by introducing additional sources of noise. It will also be useful to implement other uniform and non-uniform Hamiltonians.

*Acknowledgments.*—We would like to thank Edward (Denny) Dahl and Richard Harris of D-Wave Systems Inc. for valuable advice, technical assistance, and insightful comments on the manuscript. We also thank Adolfo del Campo, Anushya Chandran, Jacek Dziarmaga and Jonathan Wurtz for useful conversations. PW and AWS were supported by the NSF under Grant No. DMR-1710170 and by a Simons Investigator award. MT and PT were supported by the Academy of Finland under Projects No. 307418, No. 303351, and No. 318987, and by the European Research Council (ERC-2013-AdG-340748-CODE). During the later stages of this work, MT was also supported by the Polish National Science Center (NCN), Contract No. UMO-2017/26/E/ST3/00428. PW would like to thank Department of Applied Physics, Aalto University for hospitality and support during a visit. The numerical calculations were performed on the Shared Computing Cluster administered by Boston Universitys Research Computing Services.

[1] S. Lloyd, Science **273**, 1073 (1996).
[2] A. Trabesinger, Nat. Phys. **8**, 263 (2012).
[3] I. M. Georgescu, S. Ashhab, and F. Nori, Rev. Mod. Phys. **86**, 153 (2014).
[4] D. Jaksch and P. Zoller, Ann. Phys. **315**, 52 (2005).
[5] J. J. García-Ripoll, P. Zoller, and J. I. Cirac, J. Phys. B. **38**, S567 (2005).
[6] S. Diehl, A. Micheli, A. Kantian, B. Kraus, H. P. Büchler, and P. Zoller, Nat. Phys. **4**, 878 (2008).
[7] W. S. Bakr, J. I. Gillen, A. Peng, S. Fölling, and M. Greiner, Nature **462**, 74 (2009).
[8] J. Simon, W. S. Bakr, R. Ma, M. E. Tai, P. M. Preiss, and M. Greiner, Nature **472**, 307 (2011).
[9] I. Bloch, J. Dalibard, and S. Nascimbène, Nat. Phys. **8**, 267 (2012).
[10] A. Aspuru-Guzik and P. Walther, Nat. Phys. **8**, 285 (2012).
[11] A. Peruzzo, J. McClean, P. Shadbolt, M.-H. Yung, X.-Q. Zhou, P. J. Love, A. Aspuru-Guzik, and J. L. OBrien, Nat. Commun. **5**, 4213 (2014).
[12] M. J. Hartmann, J. Opt. **18**, 104005 (2016).
[13] C. Noh and D. G. Angelakis, Rep. Prog. Phys. **80** 016401 (2016).
[14] N. C. Harris, G. R. Steinbrecher, M. Prabhu, Y. Lahini, J. Mower, D. Bunandar, C. Chen, F. N. C. Wong, T. Baehr-Jones, M. Hochberg, S. Lloyd, and D. Englund, Nat. Photonics **11**, 447 (2017).
[15] N. G. Berloff, M. Silva, K. Kalinin, A. Askitopoulos, J. D. Töpfer, P. Cilibrizzi, W. Langbein, and P. G. Lagoudakis, Nat. Mater. **16**, 1120 (2017).
[16] J. I. Cirac and P. Zoller, Phys. Rev. Lett. **74**, 4091 (1995).
[17] D. James, Appl. Phys. B **66**, 181 (1998).
[18] D. Porras and J. I. Cirac, Phys. Rev. Lett. **92**, 207901 (2004).
[19] A. Friedenauer, H. Schmitz, J. T. Glueckert, D. Porras, and T. Schaetz, Nat. Phys. **4**, 757 (2008).
[20] H. Häffner, C. Roos, and R. Blatt, Phys. Rep. **469**, 155 (2008).
[21] K. Kim, M.-S. Chang, S. Korenblit, R. Islam, E. E. Edwards, J. K. Freericks, G.-D. Lin, L.-M. Duan, and C. Monroe, Nature **465**, 590 (2010).
[22] J. T. Barreiro, M. Mller, P. Schindler, D. Nigg, T. Monz, M. Chwalla, M. Hennrich, C. F. Roos, P. Zoller, and R. Blatt, Nature **470**, 486 (2011).
[23] The D-wave DW-2000Q quantum annealing device; `http://www.dwavesys.com/`
[24] R. Harris *et al.*, Phys. Rev. B **82**, 024511 (2010).
[25] R. Harris *et al.*, Phys. Rev. B **81**, 134510 (2010).
[26] N. G. Dickson *et al.*, Nat. Commun. **4**, 1903 (2013).
[27] M. W. Johnson *et al.*, Nature **473**, 194 (2011).
[28] R. Harris *et al.*, Science **361**, 162 (2018).
[29] A. Finnila, M. Gomez, C. Sebenik, C. Stenson, and J. Doll, Chem. Phys. Lett. **219**, 343 (1994).
[30] T. Kadowaki and H. Nishimori, Phys. Rev. E **58**, 5355 (1998).
[31] J. Brooke, D. Bitko, T. F., Rosenbaum, and G. Aeppli, Science **284**, 779 (1999).
[32] E. Farhi, J. Goldstone, S. Gutmann, J. Lapan, A. Lundgren, and D. Preda, Science **292**, 472 (2001).
[33] J. Roland and N. J. Cerf, Phys. Rev. A **65**, 042308 (2002).
[34] S. Suzuki and M. Okada, J. Phys. Soc. Jpn. **74**, 1649 (2005).
[35] D. R. Mitchell, C. Adami, W. Lue, and C. P. Williams, Phys. Rev. A **71**, 052324 (2005).
[36] S. Morita and H. Nishimori, J. Math. Phys. **49**, 125210 (2008).
[37] A. Das and B. K. Chakrabarti, Rev. Mod. Phys. **80**, 1061 (2008).
[38] T. Caneva, R. Fazio, and G. E. Santoro, Phys. Rev. B **78**, 104426 (2008).
[39] T. Caneva, R. Fazio, and G. E. Santoro, J. Phys. Conf. Ser. **143**, 012004 (2009).
[40] B. Heim, T. F. Rønnow, S. V. Isakov, and M. Troyer, Science **348**, 215 (2015).
[41] T. Zanca and G. E. Santoro, Phys. Rev. B **93**, 224431 (2016).
[42] S. Knysh, Nat. Commun. **7**, 12370 (2016).
[43] A. Lucas, Front. Phys. **2**, 5 (2014).
[44] M. H. Amin, E. Andriyash, J. Rolfe, B. Kulchytskyy, and R. Melko, Phys. Rev. X **8**, 021050 (2018).
[45] M. Benedetti, J. Realpe-Gómez, R. Biswas, and A. Perdomo-Ortiz, Phys. Rev. A **94**, 022308 (2016).
[46] B. Altshuler, H. Krovi, and J. Roland, PNAS **107**. (28) 12446-12450 (2010);
[47] T. F. Rønnow, Z. Wang, J. Job, S. Boixo, S. V. Isakov, D. Wecker, J. M. Martinis, D. A. Lidar, and M. Troyer, Science **345**, 420 (2014).

[48] H. G. Katzgraber, F. Hamze, and R. S. Andrist, Phys. Rev. X **4**, 021008 (2014).
[49] M. H. Amin, Phys. Rev. A **92**, 052323 (2015).
[50] H. G. Katzgraber, F. Hamze, Z. Zhu, A. J. Ochoa, and H. Munoz-Bauza, Phys. Rev. X **5**, 031026 (2015).
[51] V. Martin-Mayor and I. Hen, Sci. Rep. **5**, 15324 (2015).
[52] D. Venturelli, S. Mandr, S. Knysh, B. OGorman, R. Biswas, and V. Smelyanskiy, Phys. Rev. X **5**, 031040 (2015).
[53] J. Marshall, V. Martin-Mayor, and I. Hen, Phys. Rev. A **94**, 012320 (2016).
[54] J. Marshall, E. G. Rieffel, and I. Hen, Phys. Rev. Applied **8**, 064025 (2017).
[55] A. Mishra, T. Albash, and D. A. Lidar, Nat. Commun. **9**, 2917 (2018).
[56] V. S. Denchev, S. Boixo, S. V. Isakov, N. Ding, R. Babbush, V. Smelyanskiy, J. Martinis, and H. Neven, Phys. Rev. X **6**, 031015 (2016).
[57] N. Chancellor, G. Aeppli, P. A. Warburton, arXiv:1605.07549.
[58] B. Gardas, J. Dziarmaga, W. H. Zurek, and M. Zwolak, Sci. Rep. **8**, 4539 (2018).
[59] C.-W. Liu, A. Polkovnikov, and A. W. Sandvik, Phys. Rev. Lett. **114**, 147203 (2015).
[60] D-Wave User Manual 09-1109A-F (D-Wave Systems Inc., 2017).
[61] See Supplementary Material for further discussion of the embedding, KZM scaling in the ordered phase, additional DWQ data and analysis, TFIM with local noise source, coherence time of a single model spin, and noise generation in the model.
[62] A. Polkovnikov, Phys. Rev. B **72**, 161201(R) (2005).
[63] W. H. Zurek, U. Dorner, and P. Zoller, Phys. Rev. Lett. **95**, 105701 (2005).
[64] J. Dziarmaga, Adv. Phys. **59**, 1063 (2010).
[65] A. Polkovnikov, K. Sengupta, A. Silva, and M. Vengalattore, Rev. Mod. Phys. **83**, 863 (2011).
[66] C. De Grandi, V. Gritsev, and A. Polkovnikov, Phys. Rev. B **81**, 012303 (2010).
[67] C. De Grandi, A. Polkovnikov, and A. W. Sandvik, Phys. Rev. B **84**, 224303 (2011).
[68] C. D. Grandi, A. Polkovnikov, and A. W. Sandvik, J. Phys.: Condens. Matter **25**, 404216 (2013).
[69] C.-W. Liu, A. Polkovnikov, and A. W. Sandvik, Phys. Rev. B **87**, 174302 (2013).
[70] N. Xu, K.-H. Wu, S. J. Rubin, Y.-J. Kao, and A. W. Sandvik, Phys. Rev. E **96**, 052102 (2017).
[71] N. Xu, C. Castelnovo, R. G. Melko, C. Chamon, and A. W. Sandvik, Phys. Rev. B **97**, 024432 (2018).
[72] M. Kolodrubetz, B. K. Clark, and D. A. Huse, Phys. Rev. Lett. **109**, 015701 (2012).
[73] A. Chandran, F. J. Burnell, V. Khemani, and S. L. Sondhi, J. Phys.: Condens. Matter **25** 404214 (2013).
[74] A. Maraga, P. Smacchia, and A. Silva, Phys. Rev. B **94**, 245122 (2016).
[75] A. Dutta, A. Rahmani, and A. del Campo, Phys. Rev. Lett. **117**, 080402 (2016).
[76] A. Chenu, M. Beau, J. Cao, and A. del Campo, Phys. Rev. Lett. **118**, 140403 (2017).
[77] D. Patanè, A. Silva, L. Amico, R. Fazio, and G. E. Santoro, Phys. Rev. Lett. **101**, 175701 (2008).
[78] Z. Yan, L. Pollet, J. Lou, X. Wang, Y. Chen, and Z. Cai, Phys. Rev. B **97**, 035148 (2018).
[79] J. A. Hoyos, C. Kotabage, and T. Vojta, Phys. Rev. Lett. **99**, 230601 (2007).
[80] J. A. Hoyos and T. Vojta, Phys. Rev. Lett. **100**, 240601 (2008).
[81] K. Nishimura, H. Nishimori, A. J. Ochoa, and H. G. Katzgraber, Phys. Rev. E **94**, 032105 (2016).
[82] K. Kechedzhi and V. N. Smelyanskiy, Phys. Rev. X **6**, 021028 (2016).
[83] L. Arceci, S. Barbarino, R. Fazio, and G. E. Santoro, Phys. Rev. B **96**, 054301 (2017).
[84] M. Keck, S. Montangero, G. E. Santoro, R. Fazio, and D. Rossini, New J. Phys. **19**, 113029 (2017).
[85] D. Patané, L. Amico, A. Silva, R. Fazio, and G. E. Santoro, Phys. Rev. B **80**, 024302 (2009).
[86] P. Nalbach, S. Vishveshwara, and A. A. Clerk, Phys. Rev. B **92**, 014306 (2015).
[87] L. Arceci, S. Barbarino, D. Rossini, and G. E. Santoro Phys. Rev. B **98**, 064307 (2018).
[88] V. N. Smelyanskiy, D. Venturelli, A. Perdomo-Ortiz, S. Knysh, and M. I. Dykman, Phys. Rev. Lett. **118**, 066802 (2017).
[89] K.-W. Sun, C. Wang, and Q.-H. Chen, Europhys. Lett. **92**, 24002 (2010).